Scanning Microscopy Vol. 12, No. 1, 1998 (Pages 119-129) 0891-7035/98$5.00+.25
Scanning Microscopy International, Chicago (AMF O'Hare), IL 60666 USA

COBALT GRAIN GROWTH ON CLEAN SI(100) SURFACES

Theodore D. Lowes[1] and Martin Zinke–Allmang[2,*]

[1] JDS FITEL Inc., 570 Heston Drive, Nepean, Ontario K2G 5W8, Canada
[2] Department of Physics, The University of Western Ontario, London, Ontario N6A 3K7, Canada

(Received for publication May 15, 1996 and in revised form November 27, 1996)

Abstract

The dynamics of cobalt thin films on ultra–high vacuum clean Si(100) surfaces below the threshold temperature for silicide formation (at 375°C) is studied. We find Co grain formation and Co grain size evolution at all temperatures at and above room temperature. The clustering process is quantified with films post-deposition annealed for 15 minutes at temperatures between 250°C and 350°C. The activation energy for clustering is found to be 0.3 ± 0.2 eV, indicating that a Co surface diffusion process dominates the kinetics.

Key Words: Silicides, clustering, coalescence, electron microscopy, ion scattering.

* Address for correspondence:
Martin Zinke-Allmang
Department of Physics and Astronomy
The University of Western Ontario
London, Ontario N6A 3K7, Canada
Telephone number: (519) 661–3986
FAX number: (519) 661–2033
E–mail: mzinke@uwo.ca

Introduction

Metal silicide thin films on Si(100) have been studied in great detail for more than two decades due to the possibility to obtain self-aligned epitaxial metal-semiconductor interfaces, i.e., structures that yield superior hetero-interfaces compared to polymorphic metal deposits. Most metal silicide research is directed toward film formation at high temperatures (above 400°C) where the main driving force for structural evolution is chemical compound formation, following the sequence Co + Si → Co_2Si → CoSi → $CoSi_2$ (Lau *et al.*, 1978; Tu *et al.*, 1982; Chen *et al.*, 1991). Typical values reported for the activation energies of formation for these compounds are 1.5 – 2.1 eV for Co_2Si (Lim *et al.*, 1987), 1.8 – 1.9 eV for CoSi (Lien *et al.*, 1985; Miura *et al.*, 1991; Colgan *et al.*, 1995) and 2.3 – 2.8 eV for $CoSi_2$ (Lien *et al.*, 1984; Appelbaum *et al.*, 1985; Van den Hove *et al.*, 1986). Due to the range of activation energies, appreciable silicide formation is not observed at temperatures below 375°C (van Gurp and Langereis, 1975; Lau *et al.*, 1978; Tu *et al.*, 1982; Yalisove and Tung, 1989).

In contrast, little is known about other dynamic effects which may contribute to the final morphology, e.g., grain formation and subsequent structural ripening of the metal deposit. There is, however, indirect evidence that dynamic effects occur in the cobalt-silicon system already below the silicide formation threshold temperature. Ottaviani *et al.* (1987) and Colgan *et al.* (1995) observed minor changes in the *in situ* resistance of thin Co films on Si at temperatures in the range of 300°C to 435°C. These changes were neither correlated with silicide phase formation nor detectable diffusion of Co into the substrate. A possible explanation was offered by Colgan *et al.* based on experiments on the temperature dependence of the sheet resistance of a cobalt layer on oxidized and photoresist coated silicon in a high vacuum system (~10^{-7} torr) (Cabral *et al.*, 1993). The authors assumed that cobalt grain growth was responsible for the observed changes under these conditions, but no microscopic study of cobalt grains was provided. In molecular beam epitaxy, thin film growth is done on clean single crystal Si(100) surfaces under ultra–high vacuum conditions (10^{-9} – 10^{-10} torr), i.e., under conditions for which so far no microscopic study of Co layers below the silicide formation temperature has been reported.

The main reason why such processes are usually not

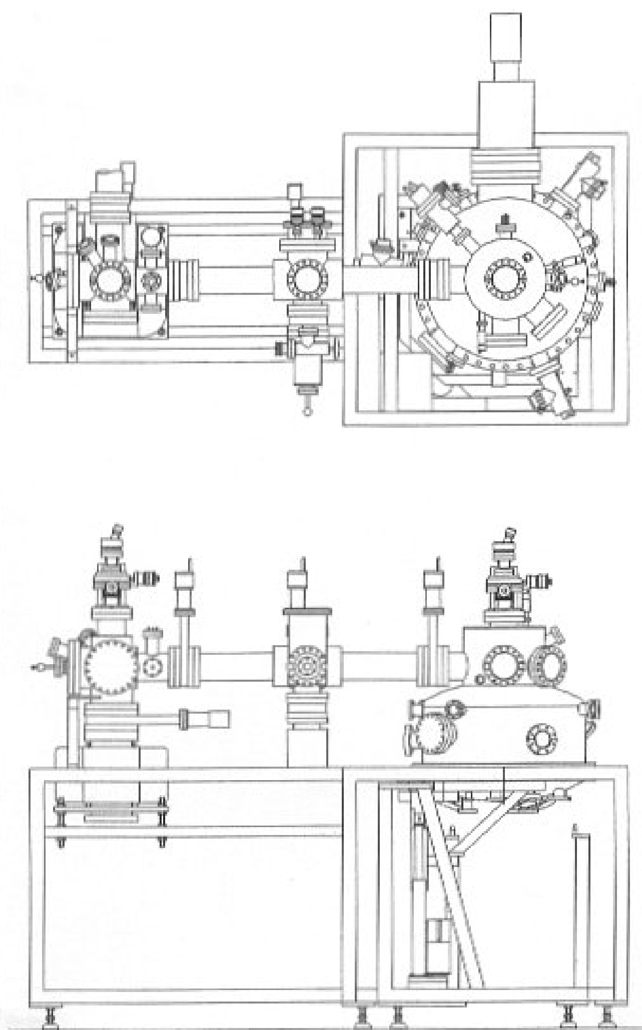

Figure 1. Top view (top) and side view (bottom) of the molecular beam epitaxial growth system (right), the sample load–lock (centre) and combined ion beam modification / ion beam analysis system (left) used in the present study.

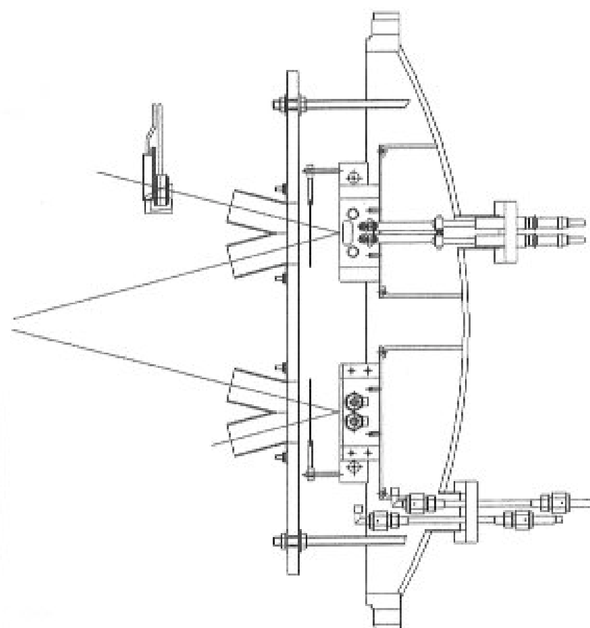

Figure 2. Side view of the sample / source arrangement in the growth system. Note the position of the quartz crystal oscillators.

studied is the general belief that they are second order effects compared to the driving force toward chemical equilibrium once silicidation starts. While this view may have been justified as long as major problems with film formation were addressed, the state–of–the–art growth capabilities for thin silicide films have significantly improved. The remaining problems, such as pinhole formation in films on Si(100) may well be attributed to "minor" causes, i.e., second order effects such as a possible propensity of deposited cobalt to cluster.

We establish through direct observation in this study the dynamics of cobalt on Si(100) under ultra–high vacuum conditions. In order to isolate these effects from concurring chemical effects, the study focuses on a thin cobalt deposit at temperatures below the processing temperatures for film formation, i.e., we discuss measurements in the range of temperatures up to 350°C. The discussion will provide a comparison with other metal layers on silicon which do not form chemical compounds with the substrate, such as tin which is immiscible with silicon.

Experimental Set–up

The films discussed in this paper were grown in a recently installed molecular beam epitaxy system at the Western Science Centre of the University of Western Ontario. Since this facility has not been described previously, its main characteristics will be reported here.

Figure 1 shows the top view (top) and side view (bottom) of the system manufactured by Kurt Lesker Co. The facility consists of two main chambers: sample characterization / ion beam modification on the left and molecular beam epitaxial growth on the right. The growth system contains three electron beam evaporation sources (two with 7 cm^3 capacity and one with 40 cm^3 capacity, manufactured by MDC, Hayward, CA) charged with Si, Ge and Co during this study and optionally three Knudsen cell evaporators mounted on a

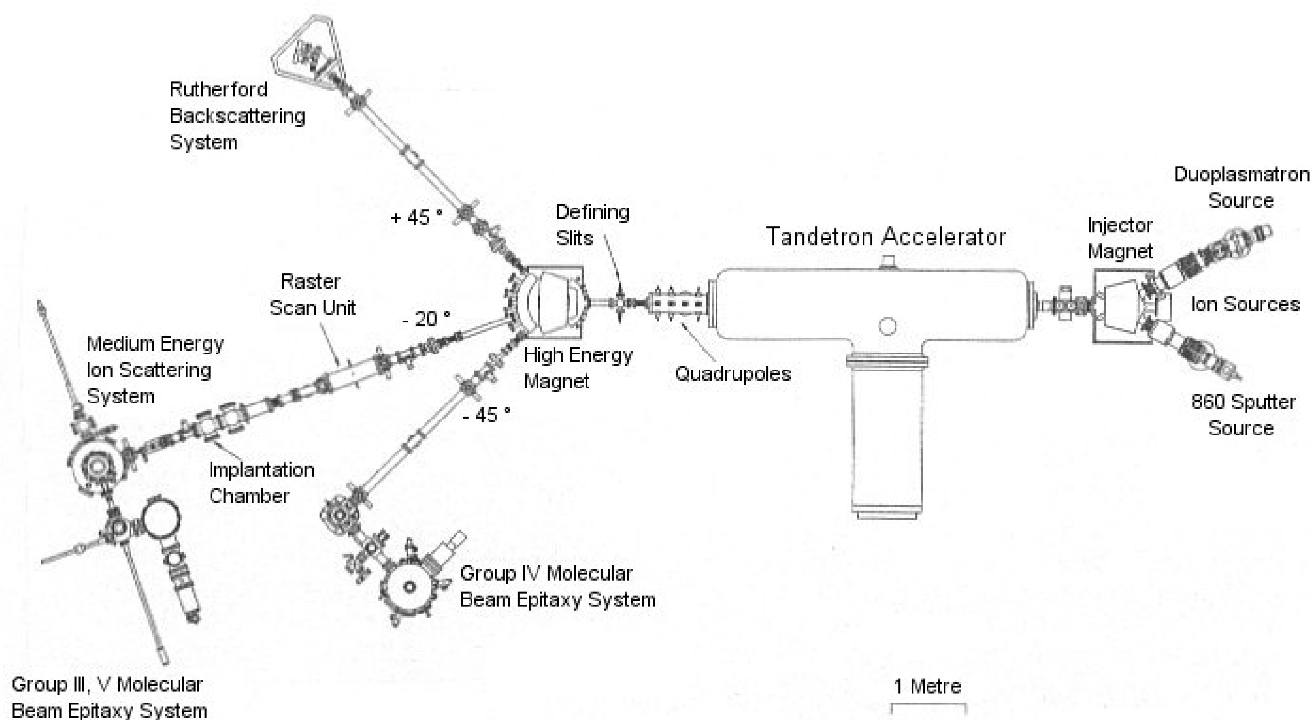

Figure 3. Floor plan of the 1.7 MV Tandetron accelerator facility at the University of Western Ontario. Three beamlines are currently active, a multi–purpose ion scattering / channeling line, a combined standard ion implantation / high depth resolution ion beam scattering line and a line leading to the system described in this paper.

large flange at the bottom of the chamber. The geometry of the deposition and thickness monitoring is shown in Figure 2. Since the quartz crystal oscillators have to be mounted at different angles and distances, calibration is required with each new source charge and is done by ion scattering analysis.

A shutter is mounted above each electron beam evaporation source for fast control of the deposition process. Above the shutter level is a plate to minimize radiative heating of the chamber walls during deposition. Water–cooling shrouds surround the chamber to guarantee a base pressure of the system of 2 x 10^{-10} torr. The sample manipulation stage is located in line of sight of all three sources and is equipped with electron beam heating capable of reaching 1100°C.

The two chambers in Figure 1 are separated to allow sample characterization and ion beam modification of films, both incompatible with the geometry and processing conditions of molecular beam epitaxy in the growth chamber. The characterization chamber can be accessed *in situ* from the growth chamber via a bidirectional transfer system. Up to eleven samples of maximum diameter of 10 mm are placed in a carousel which is transferred into the vacuum system through a load–lock (shown in centre of Fig. 1). Samples are taken from the carousel and are placed on the sample holder with a wobble stick arrangement.

Figure 3 shows the layout of the laboratory, including the accelerator facility used to provide the ion beams for ion scattering analysis and ion beam modification in the characterization chamber. Ion beams are generated by either a duoplas-matron source (for gas components) or a sputter source (usually from solid samples) and are accelerated by a 1.7 MV Tandetron accelerator. Currently, the high energy magnet provides access to three beam–lines, at +45° to a standard Rutherford backscattering/channeling facility (multi-purpose beam–line), at –20° to a standard implantation stage and a medium energy ion scattering facility for high resolution depth profiling (~ 10Å at the surface) and at –45° to the system described above. Note that the medium energy ion scattering system is in–situ connected to a second molecular beam epitaxy system featuring up to eight Knudsen cells (labelled *Group III, V MBE system*).

Experimental Results

The present study is based on thin cobalt films (nominally 60 ± 20Å thick) deposited on clean Si(100) substrates. The substrate preparation included ex–situ

degreasing and oxidation with the oxide removed during an HF dip just prior to sample mounting and transfer into the vacuum system. Samples were then outgassed and Si buffer layers of typically 50Å thickness were grown at 650°C. Finally samples were cooled to below 100°C when cobalt deposition began (Carlow *et al.*, 1995). Post–deposition annealing was done at temperatures of 250°C, 300°C and 350°C for times varying between 15 minutes and 60 minutes. After deposition and annealing, samples were analysed with ion scattering techniques (using 3 MeV He^{2+} ion beams) and transmission electron microscopy (using a Philips 100CX system; Philips Electron Optics, Eindhoven, the Netherlands) using standard ion milling procedures with Ar^{+} beams for sample preparation.

Grain size as a function of annealing temperature

The first set of data presented were prepared at varying temperatures (room temperature to 350°C) with constant annealing time (15 minutes) and nominal cobalt film thicknesses of about 60Å. Actual film thicknesses were measured by two techniques: Rutherford back scattering (RBS) and cross–sectional transmission electron microscopy (TEM). Note that both methods determine thicknesses differently and can therefore be used in combination to determine whether the Co films are incoherent, i.e., composed of isolated Co grains. The film thickness determined from RBS is based on the number of Co atoms per unit area on the surface, averaged over the analysing beam spot size (millimetre range). In contrast, cross–sectional TEM gives a direct side view of the structure with the average height of the film or the grains in the film. From the deviation between both methods the areal density of grains can be estimated. Note that a direct thickness measurement in RBS is only possible for thicknesses in excess of the detector resolution, typically starting at 150 – 200 Å. When that thickness is reached, RBS alone can be used to discuss areal density of a clustered structure.

TEM cross–sectional photographs of a sample annealed at 250°C are shown in Figures 4a–4c. The cobalt film can be identified in Figure 4a as a black stripe in centre of photograph with the silicon substrate below and TEM glue above the film. Figures 4b and 4c show the same film at higher magnification. It becomes obvious that the film is composed of a smooth layer on the silicon substrate (Si epilayer grown prior to Co deposition) and a rough granular structure which represents the Co film. The contrast variation between the silicon substrate and the silicon epilayer is due to different doping levels of the layers. RBS and cross- sectional TEM results are shown in the second and third column of Table 1 for the samples discussed in this section. The determined thicknesses differ systematically, with the nominal RBS thicknesses smaller by 73 ± 6%, i.e., again indicating an incoherent film of Co grains. The quantitative difference between the RBS and TEM thickness data will be discussed further in **Discussion**.

Figures 5a–5d show TEM diffraction patterns at the

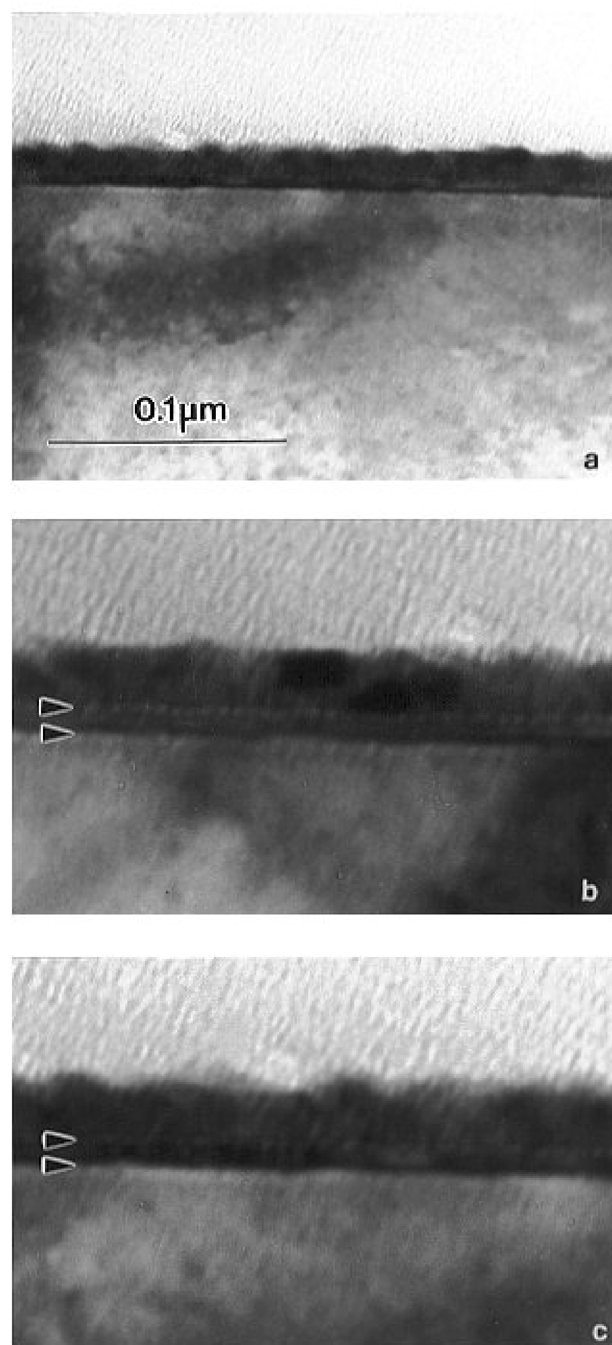

Figure 4. Cross–sectional TEM for the Co film annealed at 250°C. (**a**) Original micrograph with Si substrate bottom and TEM glue top. The Co film appears as a black stripe. (**b, c**) show two sections magnified at different contrast. Note the smooth Si epilayer (between arrows) and the granular Co film above the epilayer.

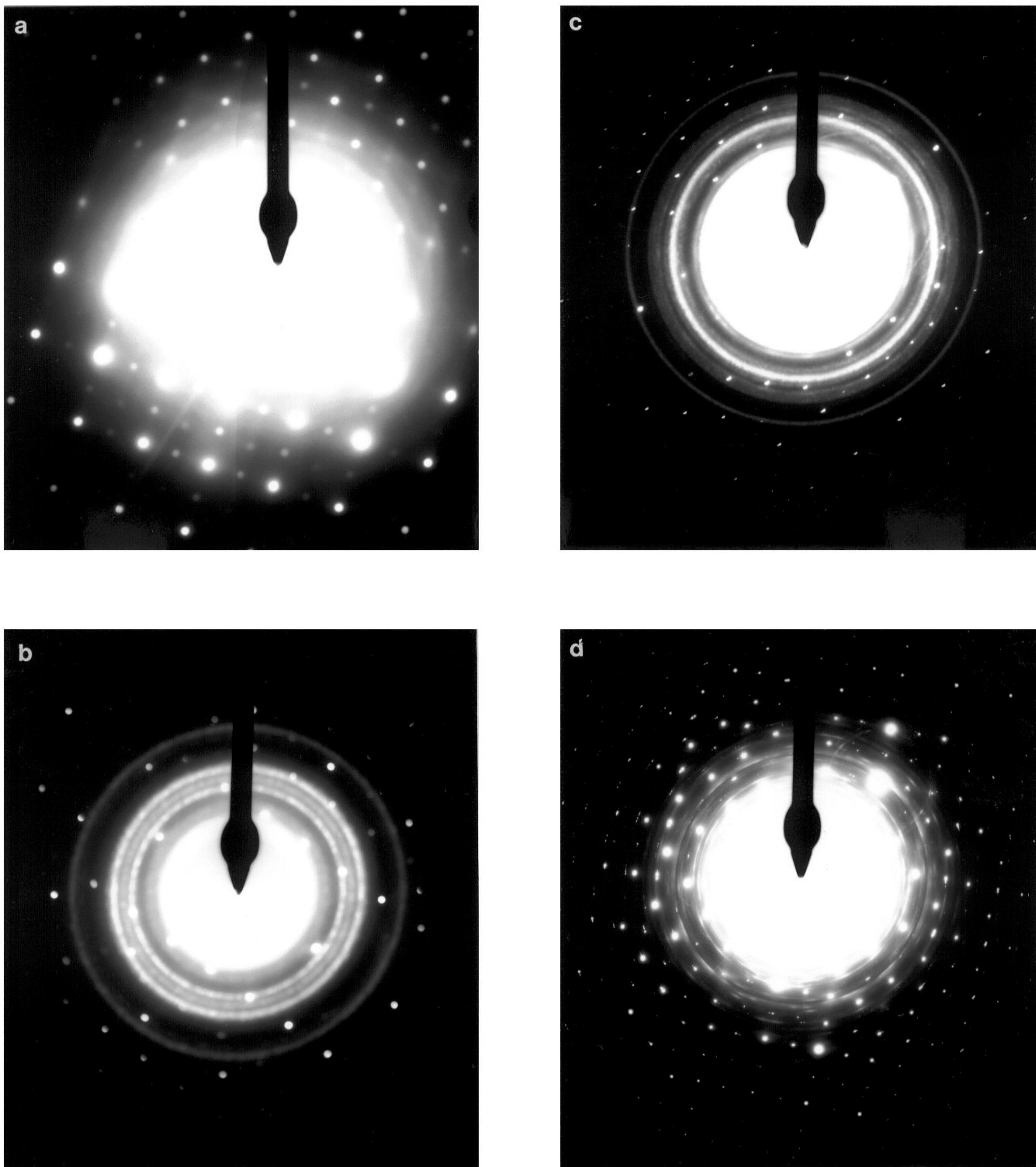

Figure 5. TEM diffraction patterns for (**a**) a room temperature sample showing an amorphous halo and a spot pattern due to the Si(100) crystal. (**b**) For the sample annealed at 250°C the halo becomes structured in diffuse rings, with the rings significantly sharper at 300°C (**c**). At 350°C (**d**) the rings are well defined and granular.

same temperatures as shown in Table 1, demonstrating the progression of pattern evolution. The room temperature sample (a) shows only an amorphous halo and a spot pattern which is associated with the underlying Si(100) crystal. The amorphous halo becomes structured into diffuse rings at 250°C (b) and at 300°C (c). At 350°C these rings are well defined and become granular indicating a propensity of the structure toward larger grain sizes with a possible trend toward texturing.

Since these diffraction patterns indicate structural changes as a function of annealing temperature, plan view TEM was used to image these structures and to quantify their typical sizes. Typical size information is not only useful as a quantitative indicator of the extent of morphological reorganization, but is also useful to determine the dynamics of the underlying growth process. Figures 6a–6d show TEM plan view micrographs of the same samples for which the diffraction patterns were given in Figure 5. Again, a progression of pattern evolution with increasing temperature is observed. Figure 6a for a sample grown at room temperature shows very small grains which become larger and better defined in Figure 6b, for the sample annealed at 250°C. As annealing temperature is increased further, to 300°C in Figure 6c and to 350°C in Figure 6d, the grains become larger and the formation of isolated clusters becomes more evident. The fourth column in Table 1 contains the typical length scale of granular structures, λ, on sets of samples as shown in Figure 6. These data are quantitatively discussed in **Discussion**.

Grain size as a function of annealing time

In a second set of experiments the time dependence of the grain growth was studied at the highest temperature used above (350°C). Deposition conditions were the same as before and the post–deposition annealing period was varied between 15 minutes and 60 minutes. Figures 7a and 7b show two structures grown at 60 minutes demonstrating a close similarity to structures grown at 15 minutes (Fig. 6d). The same quantitative analysis of the average length scale of the granular structures, as presented in the fourth column of Table 1 was done for these samples and results in 240 ± 20Å, i.e., a 25 ± 15% increase over the result at 1/4 of the annealing time.

Discussion

Figures 5 and 6 clearly indicate as a first result of this study that a thin cobalt film on a clean Si(100) surface does undergo a morphological evolution at temperatures below the threshold temperature for silicide formation, which is reported at around 375°C (van Gurp and Langereis, 1975; Lau *et al.*, 1978; Tu *et al.*, 1982; Yalisove and Tung, 1989). Cross–sectional TEM and plan view TEM indicate that a granular structure is formed. The growing grains seem to display a preferential orientation although the trend toward texturing is definitely quite incomplete in the temperature and annealing time regime studied. Further studies are required to reach conclusions on texturing of Co grains below the silicide formation threshold temperature.

Ideally one wants to study the evolution of surface structures as a function of temperature, time and initial coverage (Zinke–Allmang *et al.*, 1992). Instead, we provide TEM and RBS data to characterize the dynamic properties of a cobalt film on silicon primarily varying the temperature, but support our conclusions with some data taken as a function of time at constant annealing temperature. A more detailed study of the time dependence was not undertaken since only a typical length scale increase of less than one order of magnitude can be observed between 15 minutes and 60 minutes annealing at the highest possible temperature (Figs. 6d and 7). Establishing a power law for the dynamic process requires observation over several orders of magnitude of size and would require in the present case rather long time sequence incompatible with the experimental conditions of ultra–high vacuum studies on surfaces. We conclude therefore only qualitatively that the morphological evolution of cobalt grain growth occurs rather fast initially (i.e., in less than 15 minutes at 350°C) with a very slow progress thereafter. This implies that the time dependence of the typical length scale of the structure, λ, evolves at least as $\lambda^n \propto t$ with $n \geq 3$. Such a time dependence may be expected e.g. for diffusion limited cluster ripening (Zinke–Allmang *et al.*, 1992).

Alternatively, dynamic processes can be identified by varying the temperature at constant annealing time. While this does not provide directly the power law dependence of the structural evolution, the data can provide the activation energy of the process which may be used to characterize the microscopic rate limiting step. Although the study of cobalt structural evolution on a Si surface is again limited by the accessible temperature regime, an activation energy can be estimated from the data shown in Table 1 leading to the second, quantitative result of this study.

The typical length scale data are shown in an Arrhenius plot in Figure 8 ($\ln\lambda_{15}$ vs. 1/T with index *15* denoting that all data are taken from samples annealed for 15 minutes). Note that samples at room temperature clearly deviate from the other data. A fundamental reason for such a deviation is the occurrence of other faster processes up to a certain grain size, e.g. grain nucleation and early stage cluster coalescence, which precede grain growth. We will not attempt to quantify energy barriers involved in the nucleation process with the present data, mainly since we believe that our room temperature data points are of limited precision in temperature and time elapsed until the clustering process is terminated.

We quantify therefore the activation energy for the grain growth based on the data at elevated temperatures. The slope of the curve gives an activation energy of $E_C = 0.15$ eV. At this point, a systematic error due to the nucleation and early stage coalescence has to be corrected since the effect

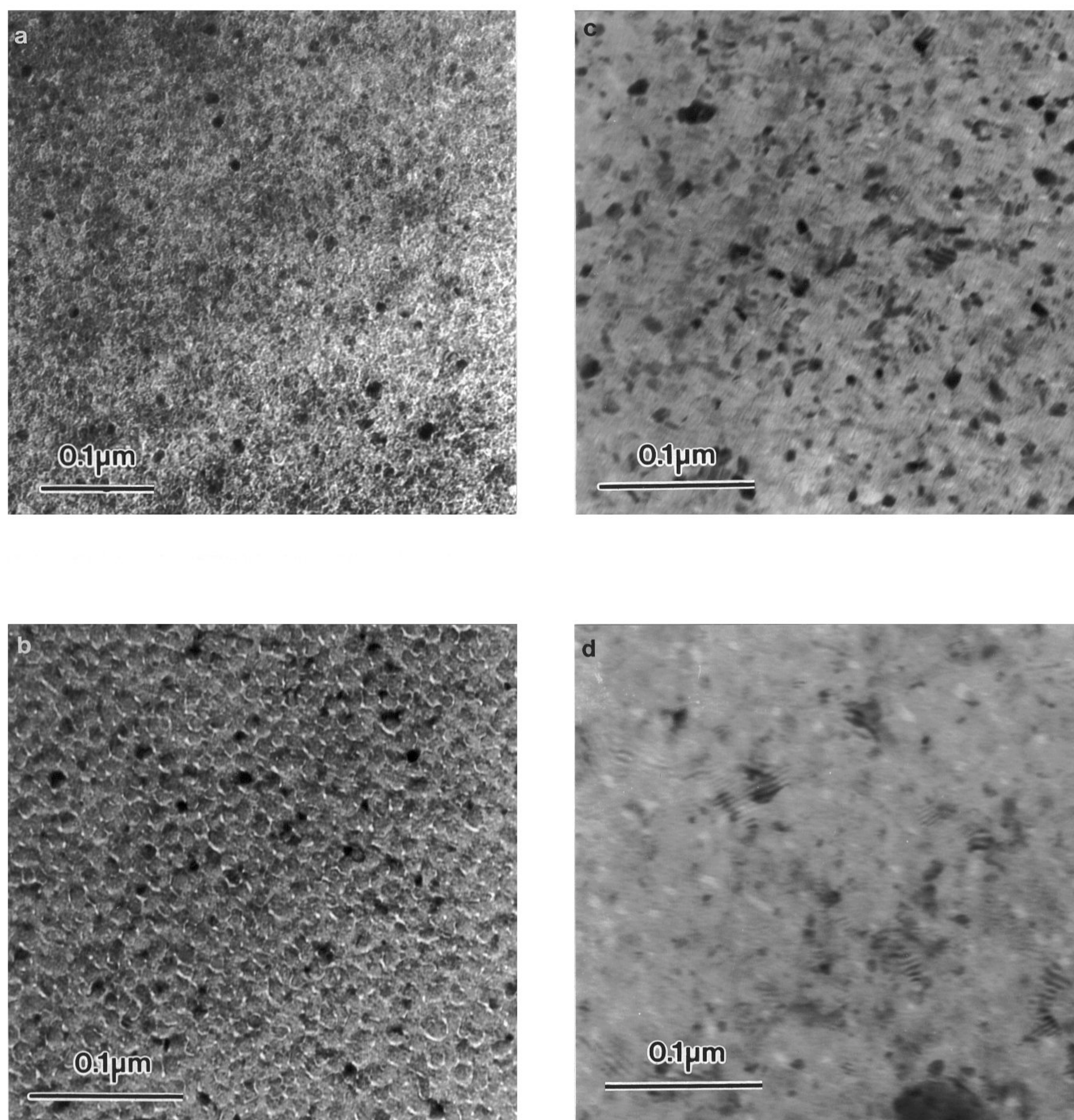

Figure 6. Transmission Electron Microscopy plan view micrographs for the same sample set for which the previous figure shows the diffraction patterns. (**a**) The sample annealed at room temperature displays very small grains. (**b**) The grains become larger and better defined for the sample annealed at 250°C. The size of the grains increases further for the samples annealed at 300°C (**c**) and annealed at 350°C (**d**). At the same time the formation of isolated clusters becomes more evident. Note the varying magnification indicated through the length bar for 0.1 µm in the bottom left corner of each micrograph.

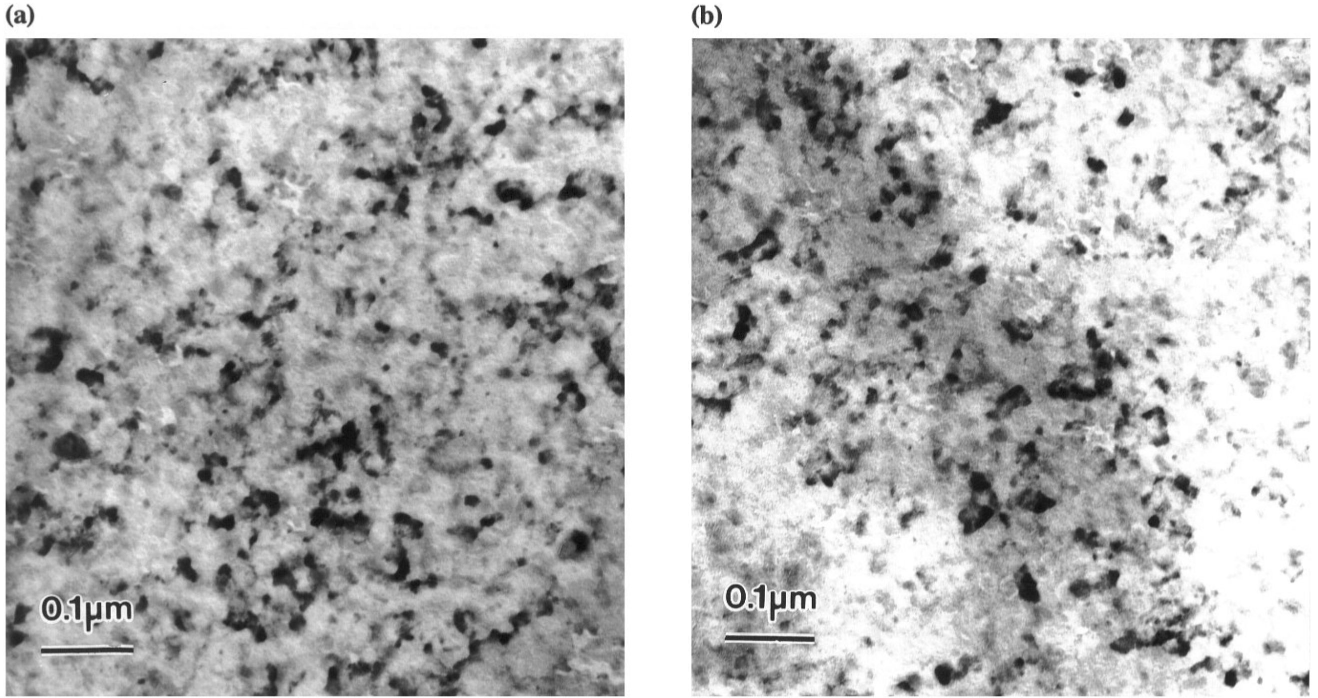

Figure 7. Two structures annealed at 350°C for 60 minutes, i.e., the same temperature but four times longer annealing time as Figure 6d. The average length scale of the granular structures is 240 ± 20Å, i.e., 25 ± 15% larger than for Figure 6d.

Table 1. Structural data from TEM and RBS for Co films post–deposition annealed for 15 minutes at variable temperatures below the threshold temperature for silicide formation. The second column shows the RBS data converted to a nominal thickness for comparison with the cross–sectional TEM data (column 3) using the density of metallic cobalt. Plan view TEM gives the lateral structure sizes in column 4.

T_{anneal} [°C] (t = 15 min)	d [Å] (RBS)	d [Å] (c.s. TEM)	λ [Å] (p. v. TEM)
RT	40 ± 3	–	90 ± 10
250	77 ± 4	100 – 110	115 ± 15
300	83 ± 5	110 – 120	140 ± 15
350	54 ± 3	70 – 80	190 ± 15

seen at room temperature is not negligible. We determine an upper limit of the activation energy by analysing a second Arrhenius plot for $\ln(\lambda - \lambda_{RT})$ vs 1/T where *RT* stands for room temperature. We report therefore a value for the activation energy of clustering for Co on Si(100) of $E_C = 0.3 \pm 0.2$ eV.

Note that we avoided carefully to label the process a "late stage" clustering process as no particular power law dependence was established (Zinke-Allmang *et al.*, 1992) and an extremely high areal coverage of Co grains may result in a prolonged transient regime toward late stage dynamics (Barel *et al.*, 1996). Thus the activation energy represents clustering in the size regime studied (several tens to few hundred Å) independently on whether it is an isolated late stage (Lifshitz-Slyozov- Wagner type) ripening process or a transient process ("early stage clustering").

This rather low activation energy can be compared to available data for the Co/Si system. Bulk diffusion of Co in Si is reported with an activation energy of 2.8 eV (Kitagawa and

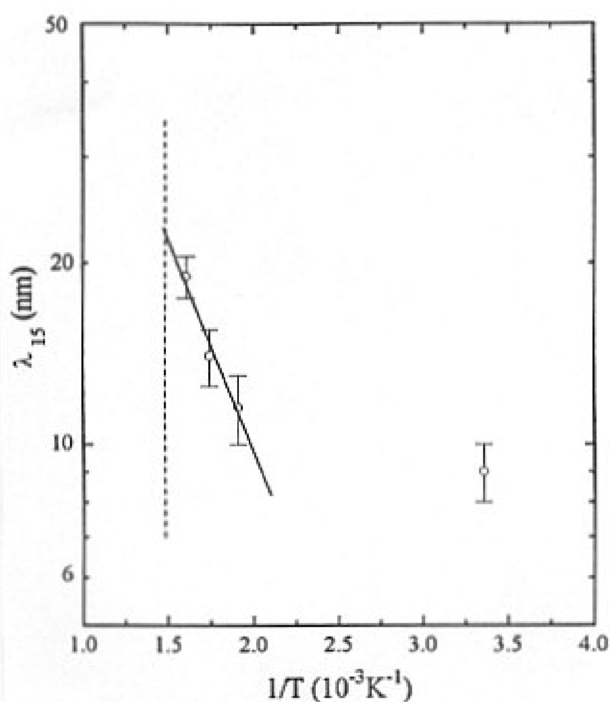

Figure 8. Arrhenius plot of typical length scales from Table 1. Note the deviation at room temperature. The slope of the curve for the data at elevated temperatures gives an activation energy of $E_C = 0.15$ eV. After correction using an Arrhenius plot for $\ln(\lambda - \lambda_{RT})$ vs 1/T, an activation energy of $E_C = 0.3 \pm 0.2$ eV is found.

Hashimoto, 1977). This clearly demonstrates that bulk indiffusion cannot be the rate determining factor for the evolution of the surface grain structure. That such a mechanism is unlikely is also obvious from the low solubility limit of Co in Si, with a maximum of 2.5×10^{16} atoms/cm³ at high temperatures (Kitagawa and Hashimoto, 1977). At such levels, electronic properties of silicon may be influenced, but morphological structure evolutions on the surface remain unaffected. Also Co bulk self–diffusion with an activation energy of 2.8 eV to 3.2 eV (Lee *et al.*, 1993), determined from radioactive tracer diffusion experiments, is not the rate limiting process.

Small activation energies usually indicate that a process is driven by surface processes rather than bulk processes. Typical clustering activation energies on Si(100) are in the range of 0.7 – 1.2 eV with some lower values, e.g. Sn/Si(-111) with 0.32 ± 0.04 eV. The low values for Sn on both Si surfaces, Si(111) and Si(100), are particularly noteworthy as Sn is also immiscible in silicon. However, tin does not form a compound with Si and clustering studies are therefore not limited to low temperatures. Sn clustering dynamics can also be observed on Si at temperatures around 200°C with initial nucleation steps already observed at room temperature (Zinke–Allmang *et al.*, 1992). Another difference between both systems is that Sn clustering occurs at temperatures where Sn is liquid and clustering proceeds with partial spherical cluster shapes representing the equilibrium (Young–Dupré) condition. Therefore the height and the width of clusters scale proportionally during cluster growth. In the present study, we observe cluster size evolution for the lateral structure size (λ) without a corresponding increase in height (from comparing RBS and cross–sectional TEM data). This can be attributed to different activation energies for the nucleation and growth of additional layers in a granular crystalline structure (Ahn and Tien, 1976).

Positively identifying the rate limiting step on the basis of the activation energy alone requires knowledge of several other activation energies, such as for surface diffusion of Co on Co and Si(100) as well as the energy of formation of Co aggre-gates. As that information is not available, other criteria have to be used to determine the mechanism of the morphological changes observed in this study. For this we rely on the combination of our RBS and cross–sectional TEM data. These data result in a description of the structure with isolated but dense Co clusters or interconnected grains with an appreciable fraction of voids, covering of the order of 75% of the surface. That conclusion is also acceptable after a detailed analysis of the plan view TEM photographs, although caution is needed as not every Co grain orientation shows the same contrast in this method. Consequently, surface diffusion of Co on Si or on a Co–Stranski–Krastanov layer on Si and the associated ripening mechanism should determine the kinetics of the clustering process. The reported activation energy is a combination of the Co bulk formation energy and the activation energy for Co surface diffusion on the uniform substrate (Zinke–Allmang *et al.*, 1992).

The results of this study are also relevant to film growth above the silicide formation threshold temperature. Undoubtedly, the propensity toward clustering of Co will determine the dynamics of free Co atoms on the surface at elevated temperatures. This will be important for a transient time until deposited Co will react with silicon to form silicide and will also play a role when locally a Co excess concentration occurs, e.g. due to fluctuations in the deposition process. The propensity toward clustering is a driving force for Co to not be available as a uniform layer for the silicidation process. This can lead to uneven layer thicknesses, as observed in titanium silicides (Ho, 1993) or may be linked to the pinhole formation in cobalt silicide layers on Si(100).

Conclusion

We have demonstrated that a Co layer on Si(100) undergoes clustering at temperatures below the silicide formation threshold temperature and as low as room temperature. The processes which cause these morphological changes have a very low activation energy ($E_C = 0.3 \pm 0.2$ eV) and are likely due to Co surface diffusion between the clusters.

Acknowledgements

We thank G.R. Carlow for some RBS data analysis and careful reading of the manuscript. A Strategic Grant from the Natural Sciences and Engineering Research Council of Canada (NSERC) is acknowledged.

References

Ahn T–M, Tien JK (1976) An extended hydrodynamic theory for particle coarsening. J. Phys. Chem. Solids **37**, 771–784.

Appelbaum A, Knoell RV, Murarka SP (1985) Study of cobalt–disilicide formation from cobalt mono-silicide. J. Appl. Phys. **57**, 1880–18-86.

Barel R, Mai Y, Carlow GR, Zinke–Allmang M (1996) Clustering on surfaces at finite areal coverages. Appl. Surf. Sci., **104/105**, 669-678.

Cabral Jr. C, Barmak K, Gupta J, Clevenger LA, Arcot B, Smith DA, Harper JME (1993) Role of stress relief in the hexagonal–close–packed to face–centred–cubic phase transformation in cobalt thin films. J. Vac. Sci. Technol. **A11**, 1435–1440.

Carlow GR, Lowes TD, Grunwell M, Zinke–Allmang M (1995) Evolution of Co/Ge films on Si(100) and Ge(100) substrates. Mat. Res. Soc. Symp. Proc. **382**, 419–424.

Chen WD, Cui YD, Hsu CC, Tao J (1991) Interaction of Co with Si and SiO_2 during rapid thermal annealing. J. Appl. Phys. **69**, 7612–7619.

Colgan EG, Cabral Jr. C, Kotecki DE (1995) Activation energy for CoSi and $CoSi_2$ formation measured during rapid thermal annealing. J. Appl. Phys. **77**, 614– 619.

Ho V (1993). Northern Telecom, Ottawa, private communication.

Kitagawa H, Hashimoto K (1977) Diffusion coefficient of cobalt in silicon. Jpn. J. Appl. Phys. **16**, 173–174.

Lau SS, Mayer JW, Tu KN (1978) Interactions in the Co/Si thin–film system. I. Kinetics. J. Appl. Phys. **49**, 4005–4010.

Lee C–G, Iijima Y, Hirano K (1993) Self-diffusion and isotope effect in face–centred cubic cobalt. Defect and Diffusion Forum **95–98**, 723–728.

Lien CD, Nicolet M–A, Lau SS (1984) Kinetics of $CoSi_2$ from evaporated silicon. Appl. Phys. **A34**, 249– 251.

Lien CD, Nicolet M–A, Pai CS, Lau SS (1985) Growth of Co–silicides from single crystal and evaporated Si. Appl. Phys. **A36**, 153–157.

Lim BS, Ma E, Nicolet M–A, Natan M (1987) Kinetics and moving species during Co_2Si formation by rapid thermal annealing. J. Appl. Phys. **61**, 5027–5030.

Miura H, Ma E, Thompson CV (1991) Initial sequence and kinetics of silicide formation in cobalt/ amorphous–silicon multilayer thin films. J. Appl. Phys. **70**, 4287–4294.

Ottaviani G, Tu KN, Psaras P, Nobili C (1987) In situ resistivity measurement of cobalt silicide formation. J. Appl. Phys. **62**, 2290–2294.

Tu KN, Ottaviani G, Thompson RD, Mayer JW (1982) Thermal stability and growth kinetics of Co_2Si and CoSi in thin–film reactions. J. Appl. Phys. **53**, 4406– 4410.

Van den Hove L, Wolters R, Maex K, De Keershaecker R, Declerck G (1986) A self–aligned cobalt silicide technology using rapid thermal processing. J. Vac. Sci. Technol. **B4**, 1358–1363.

van Gurp GJ, Langereis C (1975) Cobalt silicide layers on Si. I. Structure and growth. J. Appl. Phys. **46**, 4301–4307.

Yalisove Y, Tung RT (1989) Epitaxial orientation and morphology of thin $CoSi_2$ films grown on Si(100): effects of growth parameters. J. Vac. Sci. Technol. **A7**, 1472–1474

Zinke–Allmang M, Feldman LC, Grabow MH (1992) Clustering on surfaces. Surf. Sci. Rept. **16**, 377– 463.

Discussion with Reviewers

L. Schowalter: Surface cleanliness is crucial for experiments as reported in this paper. The present method may result in many surface contaminations, in particular in SiC precipitates, which can nucleate defects in the epitaxial Si layer. Have the authors considered this point?

Authors: We investigated the Si epilayer in plane view TEM and found no evidence for nucleation within this layer. Based on the area analysed, we can therefore report an upper limit of nucleation sites on the epilayer with 10^5 per cm^2 on the sample.

L. Schowalter: The silicide formation threshold temperature (Yalisove and Tung, 1989) is close to the highest temperature used in the present study. What evidence do the authors have that they are not forming silicides at that temperature?

Authors: We analysed carefully our TEM diffraction patterns and our RBS spectra for this point. Both techniques show no evidence of silicide formation. The RBS data, however, are close to the resolution of this technique, and we therefore emphasize the TEM diffraction data to support our conclusion.

E.A. Fitzgerald, Jr.: Do the cross–sectional TEM data in Figure 4 agree with the conclusion of a 75% coverage drawn from RBS and plane view TEM?

Authors: Qualitatively they support the concept of an

incoherent layer as structuring in the layer is visible. However, whether this indicates just misaligned grains or grains and voids cannot be concluded from cross-sectional TEM as the depth of view in transmission corresponds to the thickness of the foil (of the order of 100 nm). This is also the reason why our value for the areal cluster coverage (75%) is reported as an order of magnitude value. A slight miscut of the TEM sample may result in an overestimation of the thickness based on that method.